IAgrE Student Awards

NOMINATION SUMMARY

IAgrE CNH Industrial Award~~* / Student Project Award*~~
~~Safety Award*~~
***please delete as appropriate:**

PROPOSER: (usually Course Director/Head of Department)

Name: Graham Higginson IEng REnvP FIAgrE

Position:
Principal Lecturer Agricultural Engineering & Project Supervisor

University/College: Harper Adams University, Newport, Telford, TF10 8NB

Contact details:	**Tel:**	**Email:**
	07366 017 018	ghigginson@harper-adams.ac.uk

DETAILS OF NOMINATION:

Name of Student/Group of Students: Alexander Fuller-Shapcott

Personal contact details (i.e not college) to enable us to contact the student(s) once their course has ended:

Home Tel:	**Mob:**	**Email:**
	07901 085 721	afssweethope@gmail.com

Name of course studied: MEng Mechanical Engineering

Period studied	**From:**	**To:**
	2021	2026

Qualification to be gained: MEng Mechanical Engineering

Project Title:

Investigation of reversed agricultural tyre orientation on road-wear severity.

Details of material submitted with nomination: (Project/Exec Summary/videos etc)

Submitted project file.

SIGNED BY PROPOSER:	**DATE SUBMITTED:**
GRH	20th Oct 2026

If you wish to provide any additional information to support this nomination, please do so in a covering letter. When complete, return this form, together with the supporting documents, to

The Secretariat, IAgrE, The Bullock Building (Bldg 53), University Way, Cranfield, Bedford MK43 0GH
secretary@iagre.org

NB All work submitted is treated with complete Confidentiality; no part of the paper will be published by IAgrE except for the Title and Name of the winner in each category.



Investigation of Reversed Agricultural Tyre Orientation on Road-Wear Severity

by

Alexander J Fuller-Shapcott

E7026 Masters Engineering Project

Being a thesis submitted in partial fulfilment of the requirements for an

MEng degree in Mechanical Engineering

2026

(Word count: 9977)

MASTERS ENGINEERING PROJECT ASSESSMENT FORM

Student Declaration Form for Submission with Major Projects

Section 1

This form must be completed by the student and included at the beginning of the Masters Engineering Project.

Candidate's Name	Alexander James Fuller-Shapcott
Candidate's Number	21162200
Degree Programme	MEng Masters Mechanical Engineering
Supervisor	Graham Higginson
Major Project Title	Investigation of Reversed Agricultural Tyre Orientation on Road-Wear Severity
Word Count	9977
Confidential?	NO

In submitting this Major Project I acknowledge that I understand the definition of, and penalties for, cheating, collusion and plagiarism set out in the assessment regulations. I also confirm that this work has not previously been submitted for assessment for an academic award, unless otherwise indicated

(Electronic) Signature of student:



Date: 06/07/2026

Contents

Contents
List of Figures
List of Tables
List of Equations
Acknowledgements
Abstract i
1. Introduction 1
2. Literature Review 2
2.1 Introduction and problem context 2
2.2 Agricultural tyre use on hard surfaces 3
2.3 Contact mechanics and rubber wear variables 3
2.4 Rubber tread compound behaviour and modelling implications 4
2.5 Near-incompressibility of tread rubber in finite element models 5
2.6 Rigid-deformable road contact simplification 5
2.7 Road-going front-tyre wear mechanisms 5
2.8 Directionality and reversed lug orientation 6
2.9 Testing routes and methodological consequences 7
2.10 Research gap and project scope 8
2.11 Conclusion 10
3. Methodology 10
3.1 Methodological aim and modelling scope 10
3.2 Tyre geometry capture and CAD reconstruction 11
3.3 Building the preliminary finite element model 13
3.4 Representative tractor, tyre, and vertical load basis 14
3.5 Vertical displacement calibration 15
3.6 Simulation test matrix 16
3.7 Final material assumptions 16
3.8 Displacement-controlled loading method 17
3.9 Mesh, road proxy and contact setup 18
3.10 Contact formulation and friction model 19
3.11 Solver and contact settings 20
3.12 Model verification checks 20
3.13 Wear-severity theory and output selection 22
3.14 Output extraction and comparison method 24
3.15 Practical and ethical constraints 24
3.16 Methodology limitations 25

3.17 Methodology summary 25
4. Results 26
4.1 Post-processing basis 26
4.2 Contact status 26
4.3 Numerical comparison of tread-side contact outputs 26
4.4 Results summary 29
5. Discussion and evaluation 30
5.1 Interpretation against the research question 30
5.2 Relationship to the literature 30
5.3 Engineering significance of the result 30
5.4 Validity of the simulation evidence 31
5.5 Limitations affecting interpretation 31
5.6 Project evaluation 31
5.7 Recommendations for further work 32
6. Conclusion 32
Reference list 34

List of Figures

Figure 1 Example of standard and reversed directional agricultural tyre orientation. Source: adapted from Tires Easy (2023). 1

Figure 2 Schematic comparison of leading and trailing lug-edge loading under standard and reversed front-tyre orientation. Source: compiled by the author. 6

Figure 3 The tread lugs being coated with a water-soluble paint. Source: Author. 11

Figure 4 Painted tread footprint used to capture the agricultural lug contact outline. The 1 m steel rule was included to provide scale. Source: Author. 12

Figure 5 Scaled footprint image imported into SolidWorks and traced to create the two-dimensional tread geometry. Source: Author. 12

Figure 6 Reconstructed tread-strip geometry produced from footprint tracing and direct tyre measurement. Source: Author. 13

Figure 7 Finite element mesh of the local tread-strip contact model: (a) overall mesh layout showing the tread strip and fixed road proxy; (b) side view showing the lug geometry and tread-road contact interface. Source: Author. 18

Figure 8 Contact status comparison for the standard and reversed tyre-orientation models: (Top Left) Frame 1; reversed orientation after compression, (Top Right) Frame 2; reversed orientation after horizontal scrub, (Bottom Left) Frame 1; standard orientation after compression, (Bottom Right) Frame 2; standard orientation after horizontal scrub. Source: Author. 26

Figure 9 Tread-side Contact Traction / Tangent (Frictional Shear Mag) comparison at the final sliding frame: standard orientation; reversed orientation. Numerical comparison was based on exported tread-side values; contour plots show distribution pattern. Source: Author. 28

Figure 10 Tread-side Contact Force / Tangent (Mag) comparison at the final sliding frame: standard orientation; reversed orientation. Numerical comparison was based on exported tread-side values; contour plots show distribution pattern. Source: Author. 29

List of Tables

Table 1 Methodological synthesis mapping literature-derived constraints to simplified comparative simulation inputs. 9

Table 2 Vertical load basis used for simulation planning 15

Table 3 Vertical displacement calibration against the 10.5 kN baseline reaction target 15

Table 4 Final baseline simulation test matrix 16

Table 5 Solver and contact settings used for the final simulations. 20

Table 6 Verification checks applied to the final baseline simulations. 22

Table 7 Tread-side numerical comparison of tangential contact force and tangential traction outputs at the final sliding frame. 27

List of Equations

(Eq. 1) Local frictional power density 3

(Eq. 2) Cumulative frictional work density 3

(Eq. 3) Rated vertical force for LI133 tyre 14

(Eq. 4) Rated force for LI112 tyre 14

(Eq. 5) Becker and Els load proportion 14

(Eq. 6) Baseline vertical load scaling 14

(Eq. 7) Preliminary overload comparison 15

(Eq. 8) Summed vertical reaction force 17

(Eq. 9) Coulomb friction law 19

(Eq. 10) Archard wear expression 22

(Eq. 11) Local frictional power density 23

(Eq. 12) Cumulative frictional work density 23

(Eq. 13) Local frictional work index 23

(Eq. 14) Output extraction metrics 24

Acknowledgements

The author would like to thank the project supervisor for guidance, feedback and support throughout the project. Thanks are also given to Harper Adams University for access to the software and technical resources used during the finite element modelling work.

The author is grateful to family for access to the tractor, tyre and workshop space used during the footprint-capture stage. Appreciation is also extended to friends and peers who provided practical support and useful discussion during the project.

Abstract

Agricultural tractors increasingly operate on hard road surfaces during normal transport duties. This accelerates tread wear on lugged agricultural tyres, which were mainly designed for traction in deformable soil. A common operator practice is to reverse front tyres to improve wear uniformity, but this claim is not well supported by controlled evidence. This study investigated whether reversed agricultural front tyres reduce road-wear severity compared with standard orientation.

A Firestone Performer Extra / Performer 85 380/85R28 front tyre was used as the representative case. The tread geometry was reconstructed from a physical footprint and direct measurement, then simplified into a local tread-strip finite element contact model. The model used a fixed high-stiffness road proxy, simplified near-incompressible rubber properties and two-stage non-linear static loading. The tread was first compressed vertically into the road and then subjected to horizontal scrub displacements for the standard and reversed cases. Contact Status, Contact Force / Tangent (Mag) and Contact Traction / Tangent (Frictional Shear Mag) were used as relative wear-severity indicators.

The results showed that reversing the tread did not substantially reduce total tangential contact action. The summed tangential contact force changed by only 0.25%. However, reversed orientation reduced the peak tangential contact force by 9.25% and the peak tangential traction by 14.52%. The findings therefore suggest that reversed front tyres redistributed local wear severity rather than reduce overall road-wear loading. Further validation is required before service-life or tread-loss claims can be made.

1. Introduction

Agricultural tractors are used for both field work and road transport. Larger farms, separated land blocks and centralised storage or livestock systems mean that tractors often travel long distances on paved roads. This creates a wear problem because lugged agricultural tread patterns are designed mainly for traction and self-cleaning in soil, not repeated sliding contact on hard asphalt or concrete. On hard surfaces, tread lugs experience local contact stress, shear, braking drag and steering scrub, which can accelerate uneven wear.

A common response is to fit agricultural tyres in a reversed orientation during road use. Operators report improved wear uniformity or longer front tyre life, but the evidence is mainly experience-based. Real road use includes overlapping variables such as tyre age, inflation pressure, ballast, front-axle load, road texture, alignment, braking, steering duty, surface moisture and whether mechanical front-wheel-drive is engaged. These variables make it difficult to isolate whether reversed orientation itself changes the tread-road contact condition.



Figure 1 Example of standard and reversed directional agricultural tyre orientation. Source: adapted from Tires Easy (2023).

This project therefore investigated the question: “Do reversed agricultural front tyres reduce road wear on tractors compared with standard orientation?” The project did not attempt to measure complete tyre service life or predict tread-depth loss over a full road duty cycle. Instead, it examined whether reversing the tyre changed local wear-severity indicators at the tread-road interface. This distinction was important because tyre wear is controlled by local contact behaviour, including pressure, sliding, tangential shear and frictional work, rather than by axle load alone.

The study focused on the front tyre of a road-going tractor because front and rear agricultural tyres can experience different wear mechanisms during transport. The front tyre was physically more accessible for footprint capture and measurement. Therefore the project focused on a simplified braking or longitudinal scrub condition acting on the front tyre, rather than continuous powered wheel slip.

A Firestone Performer Extra / Performer 85 380/85R28 tyre was used as the representative tyre. The tread geometry was reconstructed from a physical footprint and direct measurement because manufacturer CAD data were unavailable. A simplified local tread-strip finite element model was

produced in Altair HyperMesh and solved using OptiStruct non-linear static analysis. The model used a fixed high-stiffness road proxy, a near-incompressible rubber material and two-stage displacement-controlled loading.

The standard and reversed cases used matched modelling conditions: the same tread geometry, mesh, material assumptions, coefficient of friction, vertical indentation and road constraint. The only intended difference was the direction of imposed horizontal scrub relative to the asymmetric lug geometry. Contact Status, Contact Traction / Tangent (Mag) and Contact Force / Tangent (Mag) were extracted from the final sliding frame as relative wear-severity indicators.

The aim was to determine whether reversed orientation produced a measurable change in local tread-side contact severity. The objectives were to reconstruct a representative agricultural tread geometry, develop a stable non-linear contact model, calibrate vertical indentation to a representative front-wheel load, compare standard and reversed orientations under equal and opposite scrub, and evaluate whether the results supported the practical claim that reversed front tyres reduce road wear.

2. Literature Review

2.1 Introduction and problem context

Modern agricultural logistics required tractors to travel between separated fields, yards and central facilities. Becker and Els (2022) documented this shift, attributing it to larger farms and greater travel on non-deformable asphalt. For lugged agricultural tyres, this created a hard-surface wear mechanism different from the soil interaction for which the tread geometry was primarily optimised (Becker and Els, 2022; Sakhnevych and Genovese, 2024; Liu and Cebon, 2025).

To reduce replacement costs, operators fitted tyres in a reversed orientation during extended road transport, claiming improved wear uniformity and longer life (The Farming Forum, 2016). These reports were useful as a starting point, but uncontrolled, as they mixed front and rear tyres, powered and free-rolling axles, tyre age, inflation pressure. This investigation targeted the front axle exclusively. Unlike the rear axle, which remained continuously driven to provide primary tractive force, the front axle on a road-going tractor typically operated with mechanical front-wheel drive (MFWD) disengaged. The front tyres functioned primarily as unpowered tracking elements, isolating the wear mechanics to steering alignment scrub and braking drag. Because The Farming Forum (2016) claims mixed front and rear tyres, the project therefore restricted the simulation to a front-tyre road-scrub case.

The scope focused on whether reversal changed local tread-block kinematics and frictional work distributions under simulated transport states (Cho, Choi and Kim, 2011; Nguyen *et al*., 2018; Liu and Cebon, 2025). Tread reversal was therefore treated as a possible wear-redistribution mechanism, not as an assumed reduction in total material loss (The Farming Forum, 2016; Nguyen *et al*., 2018; Becker and Els, 2022).

The literature was stronger on general tyre wear than on reversed agricultural tyres on paved roads. Becker and Els (2022) showed that hard-surface agricultural tread loss changed tyre stiffness and traction response, while wider tyre-wear studies linked severity to pressure, sliding, frictional work, temperature, roughness and directional damage history (Nguyen *et al*., 2018; Becker and Els, 2022; Sakhnevych and Genovese, 2024; Liu and Cebon, 2025). No peer-reviewed study was found that directly compared identical agricultural front tyres in standard and reversed orientation on a hard road surface.

2.2 Agricultural tyre use on hard surfaces

Becker and Els (2022) provided the closest agricultural evidence because their work addressed lugged agricultural tyres on asphalt and other non-deformable surfaces. This made hard-surface operation a relevant agricultural problem rather than a road-vehicle analogy.

Their results showed that as tread was removed, tyre stiffness, traction response and vehicle-level behaviour changed, meaning that tread condition had to be treated as a mechanical variable rather than a cosmetic measure of remaining life.

This mattered because agricultural tread lugs form a large structural part of the tread, not a thin surface pattern. Tread loss can change local stiffness, contact pressure and load transfer, so a reversed-orientation comparison had to treat the lug as a load-bearing contact feature rather than a simple directional pattern.

The test programme used a Trelleborg TM700 280/70R16 agricultural lug tyre at 100%, 50% and 0% tread, with two inflation pressures and one 5.68 kN load case (Becker and Els, 2022). That load was lower than the likely front-wheel load of a larger road-going tractor, so the numerical values could not be transferred directly to this project. The useful contribution was narrower: under controlled hard-surface conditions, tread state changed the mechanical behaviour of an agricultural tyre.

Becker and Els (2022) did not test standard versus reversed orientation, but their work set an important control requirement. Tread state, inflation pressure and contact condition had to be matched; otherwise, any orientation effect could have come from tread-depth change, altered contact patch shape or stiffness variation.

2.3 Contact mechanics and rubber wear variables

Tyre wear operated as a localised tribological phenomenon dependent on discrete boundary interactions rather than macro-scale parameters like gross axle load or cumulative rolling distance. The main variables were contact pressure, tangential shear distribution, slip velocity, substrate macro-texture, temperature and polymer viscoelastic properties. Sakhnevych and Genovese (2024) treated tyre wear as a multi-physical system coupling rubber behaviour, road topology. This model evaluated material character as a function of excitation frequency and thermal state, addressing the non-linear behaviour of elastomers under cyclic rolling conditions.

Classical engineering abstractions correlated wear intensity with frictional power or work densities, a method requiring precise definition of local sliding boundary states. Localised frictional power density was defined via the product of tangential traction and slip velocity:

$$\dot{w}_f = \tau_t v_s$$

(Eq. 1)

where denoted local tangential traction and denoted local sliding velocity. Integration across a discrete contact interval yielded the cumulative frictional work density:

$$w_f = \int \tau_t v_s dt$$

(Eq. 2)

These expressions were not used for absolute wear prediction because material-specific wear constants, thermal evolution and measured tread removal were not available. Their value was to

identify tangential traction and sliding as better comparative indicators than gross reaction force alone.

Liu and Cebon (2025) argued that wear models must connect contact mechanics to mass loss, but standard Archard-type approaches remain limited for elastomeric tread wear because rubber deformation, asperity interaction and micro-tearing do not behave like simple adhesive wear.

Gross reaction force was therefore a weak wear indicator when considered in isolation. More useful outputs were local contact state, tangential traction and, where sliding velocity was defined, frictional work or power density.

Road texture further limited any simple load-based interpretation. Rubber friction depended on deformation over asperities, with hysteresis and adhesion both affected by pavement texture and tread-compound behaviour (Moore, 1972; Kane and Cerezo, 2015; Vieira *et al*., 2015). For a lugged agricultural tyre on asphalt, the contact severity was shaped by how each lug edge entered contact, deformed under load, slid locally and released from the road surface.

Temperature was a limitation. Sakhnevych and Genovese (2024) linked temperature gradients to stress, strain and damage in tread compounds, but thermal evolution was not modelled here. Orientation effects therefore had to be interpreted as relative contact-severity differences, not heat-driven wear predictions.

2.4 Rubber tread compound behaviour and modelling implications

Rubber tread behaviour could not be treated as a simple linear material. Tyre tread compounds are proprietary blends whose exact formulation, filler content and cure state are not normally available. Published studies therefore tend to treat tread rubber through measured mechanical behaviour, simplified material models or representative laboratory compounds rather than exact commercial tyre recipes.

Tread compounds used in tyre-wear studies commonly include styrene-butadiene rubber (SBR) based formulations because SBR compounds are widely used where abrasion resistance, friction behaviour and heat build-up are important. Plaschka *et al*. (2025), for example, compared two carbon-black-filled SBR tread compounds under dynamic abrasion and showed that compound stiffness, hysteresis, cross-linking and test mode could alter both friction response and wear ranking. This confirmed that tread wear is strongly compound-dependent and that a material value used in simulation cannot be assumed to represent a specific commercial tyre unless it has been calibrated against that tyre.

Agricultural tread lugs add a further complication because they are not thin passenger-car tread ribs. They are large load-bearing features that must survive field traction, road abrasion, chip damage and repeated bending. The exact Firestone tread compound used in this project was not available, so the later finite element model could not claim to use a calibrated Firestone material. The literature instead justified a controlled comparative assumption: the same representative rubber stiffness had to be applied to both standard and reversed cases so that orientation, rather than material variation, remained the independent variable.

This distinction affected the interpretation of the simulation. A simplified elastic material could support a relative comparison of local contact severity if it was applied consistently, but it could not predict absolute tread-depth loss, heat generation, ageing, crack growth or rubber mass loss. The

material model therefore acted as a controlled modelling input, not as a complete description of the tyre compound.

2.5 Near-incompressibility of tread rubber in finite element models

Vulcanised rubber is usually treated as nearly incompressible in finite element contact models because it deforms mainly by shape change rather than volume change. Under compressive contact, this is commonly represented by a Poisson's ratio close to 0.50, with a value slightly below 0.50 used to avoid numerical difficulty.

The use of nu = 0.49 was consistent with simplified numerical rubber-tread modelling. Licher *et al*. (2023) used a rubber Poisson's ratio of 0.49 in a tyre-tread wear model and noted that rubber parameters depend on temperature and load frequency. This supported nu = 0.49 as a modelling assumption, not as calibrated Firestone compound data.

2.6 Rigid-deformable road contact simplification

The road body can be simplified when the modelling aim is rubber deformation rather than pavement deformation. In hard-surface transport, tread rubber is much more compliant than the road, so the main deformation of interest is in the lug and interface response.

In finite element terms, this was a contact problem in which the interface condition could change as the surfaces opened, closed, stuck or slipped relative to one another. Wriggers (2006) describes computational contact as a boundary non-linearity governed by the changing interaction between contacting surfaces. This supported the use of a defined tread-road contact formulation rather than treating the road interface as a simple fixed support.

The rigid-road simplification is consistent with tyre-road friction modelling literature. Kane and Cerezo (2015) modelled a rubber friction element against a road profile and treated the road as a rigid semi-infinite body. Their work still showed that road texture is important, because texture affects rubber deformation, hysteresis and friction generation. The useful point for this project is that a rigid or high-stiffness road body can be a defensible simplification when the model is focused on rubber response.

The later finite element model used a high-stiffness road proxy for the same reason. This allowed the tread lug to be the deforming body while the road acted as the controlled counter-surface. The simplification improved comparison control between the standard and reversed cases because both orientations interacted with the same road representation. However, it limited physical realism because real asphalt and concrete surfaces contain macro-texture, micro-texture, aggregate shape, debris, moisture and temperature variation.

The high-stiffness road proxy was therefore acceptable for a controlled orientation comparison, but it could not represent full real-road friction and wear behaviour. Results had to be interpreted as relative contact-severity indicators under matched hard-surface assumptions.

2.7 Road-going front-tyre wear mechanisms

For road transport, the front tyre had to be treated differently from a powered rear tyre. Rear tyres can experience engine-driven slip, while a front tyre on a road-going tractor are normally steered and free-rolling when MFWD is disengaged. John Deere (2018) recommended disengaging MFWD

during road travel to improve front tyre life. Relevant front-tyre road mechanisms were therefore braking drag, steering or alignment scrub, lug compression and shear release.

The analysis therefore focused on local wear-severity indicators rather than whole-vehicle traction. Reversal changed which lug face became the leading or trailing edge during scrub, so the effect could not be inferred from axle load or speed alone.

2.8 Directionality and reversed lug orientation

After the front tyre was defined as a scrubbed road-contact case, direction-dependent abrasion became the main mechanism linking orientation and wear. Nguyen *et al*.(2018) showed that abrasion models based only on pressure and sliding velocity were incomplete because they ignored sliding history, directional effects and flash temperature.

Geometric reversal of an agricultural tyre transposes the leading and trailing lug faces relative to the primary velocity vector, altering the localised deformation timeline across the contact patch. This high-aspect-ratio lug geometry was fundamentally optimised for shear engagement and self-cleaning performance within deformable macro-topographies (Ally *et al*., 2025; Marques Filho *et al*., 2025). When operated on a rigid, non-deformable substrate, this inherited geometry induces severe strain concentrations at the localised boundaries, governed by the interaction of instantaneous scrub directions, normal contact pressures, and historical loading profiles (Nguyen *et al*., 2018; Sakhnevych and Genovese, 2024; Liu and Cebon, 2025). This orientation-dependent boundary shift is illustrated schematically in Figure 2.

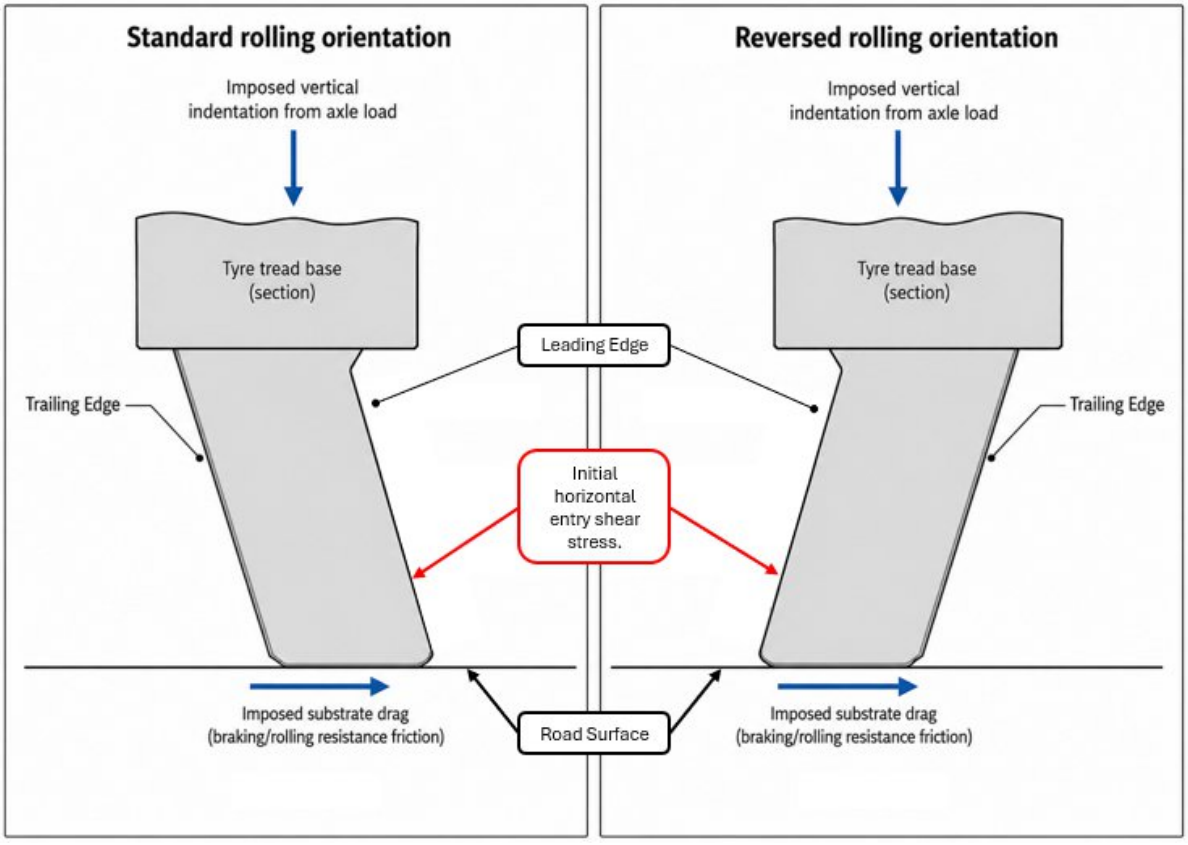


Figure 2 Schematic comparison of leading and trailing lug-edge loading under standard and reversed front-tyre orientation. Source: compiled by the author.

Nguyen *et al*. (2018) linked abrasion pattern development and wear rate to sliding direction and contact history. Their discussion of Schallamach-type abrasion showed that unidirectional sliding

generated ridge patterns associated with the abrasion direction, while changes in sliding direction changed the wear response. That evidence did not prove a service-life benefit for reversed agricultural tyres. It supported a narrower engineering expectation: orientation could change wear distribution because each lug edge experienced a different scrub direction and damage history.

The important distinction was between reducing total wear and redistributing wear. Reversal might reduce peak wear at one lug edge while increasing wear elsewhere, so the tread could look more even without losing less rubber overall. The effect could be beneficial under braking drag but unfavourable under turning, alignment scrub or MFWD assisted road use. For that reason, the project tested local wear-severity indicators rather than claiming that reversed tyres had longer life durability.

2.9 Testing routes and methodological consequences

The reviewed literature supported simulation as a useful first route because tyre orientation could be changed while tread geometry, load, material assumptions and road-contact conditions were held constant. However, simulation alone could not prove tyre-life improvement.

Becker and Els (2022) showed that tyre models were only as useful as their input data, particularly when tyres provided the main excitation into the vehicle model. For this project, that meant geometry, load, inflation pressure, friction and contact behaviour could not be treated as minor details. Poorly defined inputs would have made the model look precise while leaving it physically weak (Becker and Els, 2022; Liu and Cebon, 2025).

Finite element and wear-modelling studies showed why simulation suited a narrow comparison. Braghin *et al*. (2005) linked tyre-wear prediction to local frictional power under defined vehicle and manoeuvre conditions, while Cho, Choi and Kim (2011) used 3D patterned-tyre rolling analysis to calculate frictional energy rates and estimate abrasive wear. These studies did not remove the need for validation, but they showed that simulation could isolate a chosen variable when the boundary conditions were stated clearly (Braghin *et al*., 2005; Cho, Choi and Kim, 2011; Farroni and Sakhnevych, 2022).

Small-scale wear rigs and road tests were considered, but both had control limitations. Wear rigs were useful for studying mechanisms, although Huang *et al*. (2018) showed that debris in the contact zone changed measured wear rate, while Plaschka *et al*. (2025) showed that conventional laboratory tests often failed to reproduce transient tyre-road contact. Full-scale road testing would have been more realistic, but it would have introduced many variables that could mask orientation effects, including road texture, temperature, inflation pressure, steering input, ballast, braking, moisture and wheel alignment (Sakhnevych and Genovese, 2024; Giechaskiel, Ferrarese and Grigoratos, 2025; Zhang *et al*., 2025). These options would have strengthened the work only if load, sliding, debris, temperature and contact timing were tightly controlled.

A simulation-led method was therefore appropriate because the research question was narrow: whether reversed orientation changed local wear-severity indicators under matched conditions. Physical or road testing would have strengthened the study, but only if the main wear variables could be controlled closely enough to isolate tyre orientation.

2.10 Research gap and project scope

The literature narrowed the project to an unresolved overlap between agricultural front-tyre mechanics and tyre-wear tribology. Agricultural studies showed that hard-surface tread loss changed tyre behaviour, while wear studies linked abrasion to local pressure, sliding, shear, frictional work, temperature and damage history.

The evidence did not establish the common operating claim that reversing agricultural front tyres reduced road wear. No peer-reviewed study was identified that directly compared identical front agricultural tyres in standard and reversed orientation under paved-road tractor transport conditions.

The gap existed because agricultural tyre studies mainly addressed traction, soil compaction, stiffness, inflation pressure and tyre-road or tyre-soil response, rather than orientation-dependent wear during paved-road transport while general tyre-wear studies usually used passenger-car tyres, truck tyres or laboratory rubber specimens rather than agricultural lug geometry (Becker and Els, 2022; Liu and Cebon, 2025; Zhang *et al*., 2025).

The review set four constraints for the method. The standard and reversed cases required matched tread state, vertical loading, material assumptions and road-contact conditions. The front tyre had to be treated as a scrubbed road-contact case, outputs had to focus on local contact status and tangential traction, and interpretation had to remain limited to relative contact severity unless validated wear data were added. Table 1 summarises this translation into the final comparative model.

Table 1 Methodological synthesis mapping literature-derived constraints to simplified comparative simulation inputs.

Parameter category	**Field operational baseline**	**Simulation representation method**	**Underlying literature justification**
Tyre orientation	Standard and reversed front-tyre fitting during road transport	Matched standard and reversed cases compared using the same tread geometry	Reversal changes the local leading/trailing lug-edge contact history, but no direct peer-reviewed agricultural front-tyre comparison was identified.
Vertical loading	Representative front-wheel load during road transport	Displacement-controlled vertical indentation, calibrated to a target reaction force	Local contact pressure is central to tread wear severity, so vertical loading had to be controlled rather than left arbitrary.
Horizontal action	Braking drag, free-rolling scrub, steering/alignment effects on an unpowered front axle	Equal and opposite imposed horizontal scrub displacement	Represents road-going local scrub rather than continuous driven front-wheel spin.
Material behaviour	Proprietary non-linear tread compound with viscoelastic and temperature-dependent behaviour	Same simplified near-incompressible elastic rubber assumption used for both cases	Exact commercial tread data were unavailable, so material variation was controlled rather than used as an independent variable.
Near-incompressibility	Rubber tread deforms mainly by shape change rather than volume change	Poisson's ratio close to 0.50 used in the finite element material definition	Supports realistic rubber-like contact deformation while maintaining numerical stability.
Road-contact body	Hard paved surface or concrete yard condition	Fixed high-stiffness road proxy	Allowed the tread lug to act as the main deforming body while keeping the road-contact condition matched between orientations.
Contact interpretation	Local contact opening, sticking and sliding at lug-road interface	Contact Status, Contact Traction / Tangent (Mag), and Contact Force / Tangent (Mag)	Local contact state and tangential traction are more relevant to wear severity than global force alone.
Wear prediction boundary	Real tyres lose tread depth and mass over repeated duty cycles	Relative wear-severity indicators only; no absolute material removal calculation	No calibrated wear law, thermal model or full road-duty cycle was implemented, so results cannot predict service life or mileage.

2.11 Conclusion

The reviewed literature did not establish that reversing agricultural front tyres increased service life during road transport. No direct peer-reviewed comparison was identified for identical front agricultural tyres in standard and reversed lug orientation on a paved-road duty cycle.

The hypothesis remained mechanically plausible because wear was governed by local sliding, tangential shear, frictional work, road texture, temperature and damage history. Reversing the tread changed which lug edge received the leading and trailing contact history.

The project was therefore framed as a controlled comparison of local wear-severity indicators under road-going conditions. It did not claim absolute tread-depth loss, rubber mass loss, mileage or whole-life economy.

3. Methodology

3.1 Methodological aim and modelling scope

The methodology used a simplified, quasi-static tread-road contact model to evaluate local tread-road interface behaviour. It did not attempt to model a full rolling tyre, pneumatic carcass or progressive mass loss. Instead, it isolated one tread-strip contact event, consistent with literature showing that elastomer wear is governed by local pressure, sliding, shear traction and frictional work rather than gross wheel load alone (Cho, Choi and Kim, 2011; Sakhnevych and Genovese, 2024; Liu and Cebon, 2025).

The simulation was restricted to the front tyre of a road-going agricultural tractor. Rear tyres may experience engine-driven torque slip, while front tyres normally acted as tracking, steering and braking tyres when MFWD was disengaged on paved surfaces. The model therefore represented longitudinal braking scrub on the front tyre rather than powered front-wheel slip.

3.2 Tyre geometry capture and CAD reconstruction

The tread geometry was reconstructed from the physical Firestone Performer Extra / Performer 85 380/85R28 tyre because manufacturer CAD data were unavailable. The workshop floor and tread were cleaned, the lugs were coated with water-soluble paint (Figure 3), and the tractor was rolled slowly across dry concrete to capture the lug footprint.



Figure 3 The tread lugs being coated with a water-soluble paint. Source: Author.

A 1 m steel rule was included in the photograph to provide scale (Figure 4). The image was imported into SolidWorks using Sketch Picture (Figure 5), scaled from the rule, and manually traced to create the two-dimensional tread-lug boundary. Direct measurements from the tyre were then used to define tread depth, draft angle, local radii and under tread thickness.



Figure 4 Painted tread footprint used to capture the agricultural lug contact outline. The 1 m steel rule was included to provide scale. Source: Author.

The footprint came from a mounted tyre, so the outline included the tyre condition at measurement, including inflation pressure and deflection. However, inflation pressure was not an independent simulation input because the carcass and air cavity were excluded.

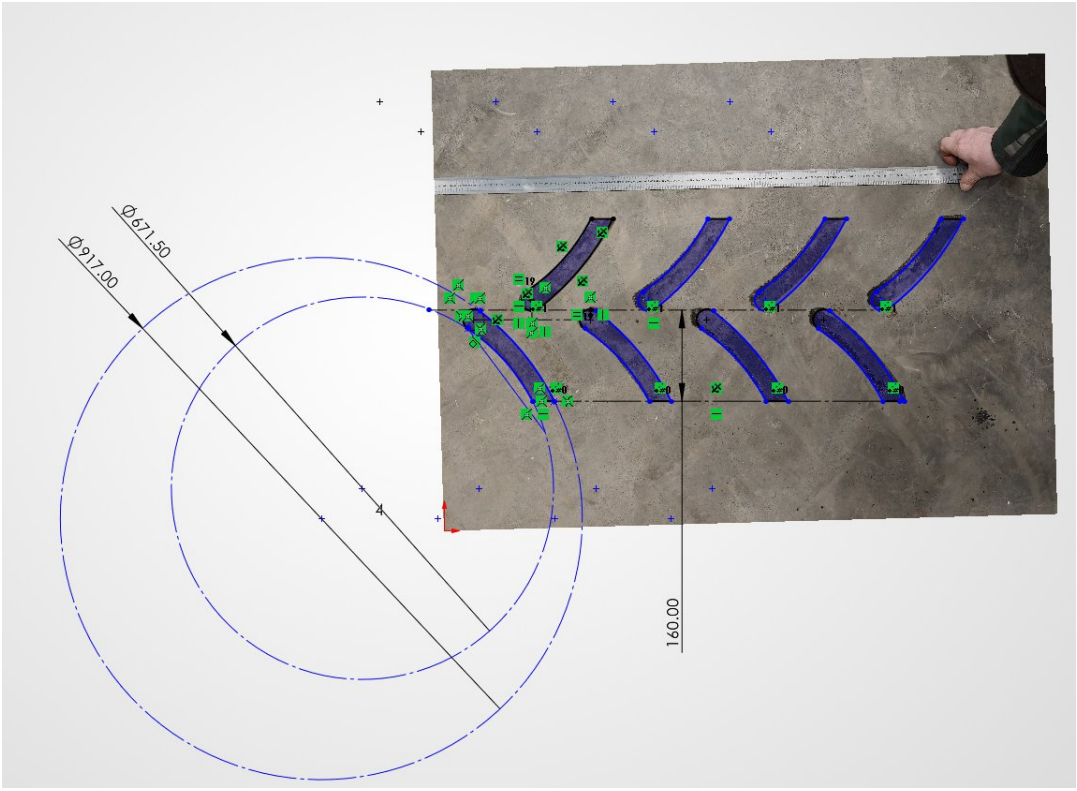


Figure 5 Scaled footprint image imported into SolidWorks and traced to create the two-dimensional tread geometry. Source: Author.

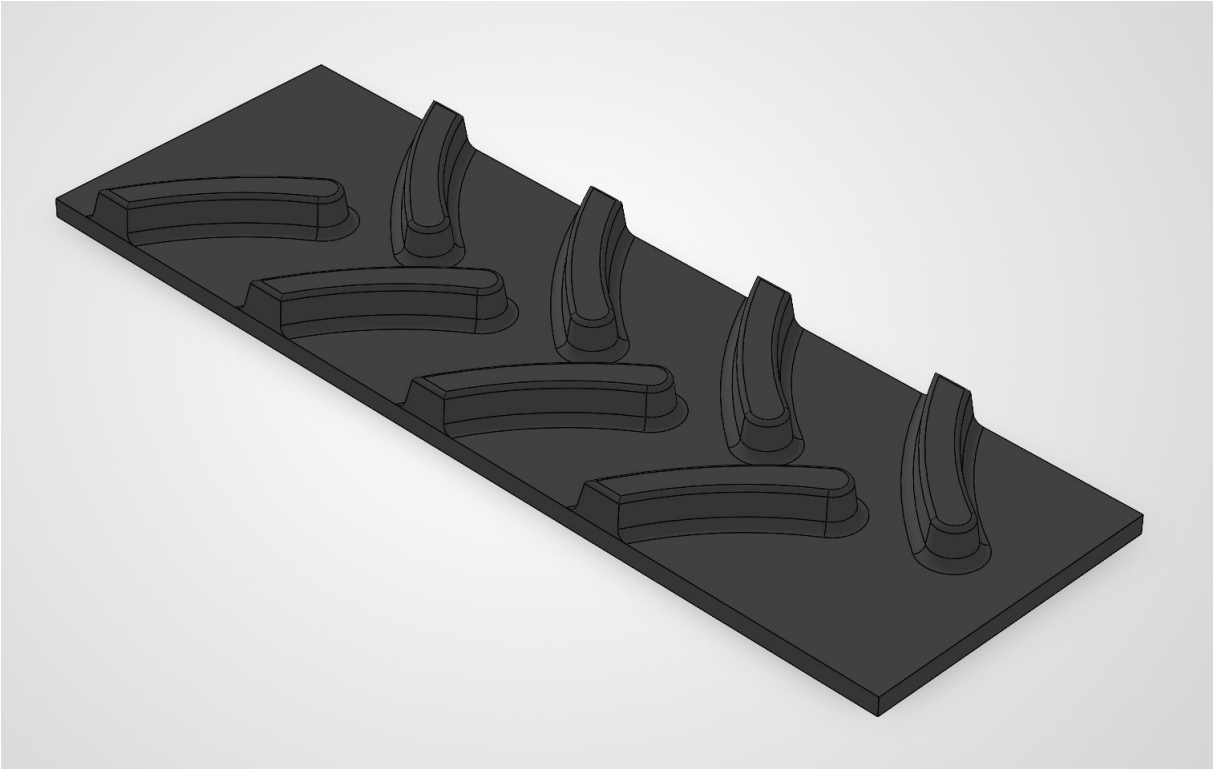


Figure 6 Reconstructed tread-strip geometry produced from footprint tracing and direct tyre measurement. Source: Author.

The final CAD model (Figure 6) represented a local tread strip suitable for comparing standard and reversed orientation under matched contact conditions. It did not reproduce a full tyre carcass, belt package, sidewall, bead region or air chamber. This was deliberate: the model needed enough geometric realism to represent the lug contact shape, but not the complexity of a full tyre model.

3.3 Building the preliminary finite element model

The preliminary finite element model checked whether the reconstructed tread could form stable contact with a hard road and produce usable outputs. It was a solver-development stage, not the final standard-versus-reversed comparison.

The model was prepared in Altair HyperMesh and solved using OptiStruct non-linear static analysis. It used a tread strip, fixed stiff road block and the initial rubber material of E = 7.5 MPa and nu = 0.49 to establish contact stability rather than an exact Firestone tread compound.

Early trials showed that the tyre-road contact could not be set up reliably by applying all loading in one step. When normal compression and horizontal scrub were applied together, the model was more likely to fail before a stable contact patch had formed. The model was therefore developed with enforced displacement: vertical movement established contact first, then horizontal movement applied local scrub.

The vertical displacement input was labelled D2. A value of D2 = -2.8 mm was used in the first working contact model. This value successfully created contact and allowed the main contact outputs to be extracted, including Contact Status, Contact Traction / Tangent (Mag), and Contact Force / Tangent (Mag). However, the summed vertical reaction force from this setup was approximately 22.06 kN.

This reaction force showed that the preliminary indentation was too severe for the intended representative front-wheel baseline. The selected Firestone 380/85R28 tyre has a load index of

133, equivalent to approximately 2060 kg or 20.2 kN per tyre at its rated load condition. The preliminary reaction of 22.06 kN was therefore above the rated-load basis and could not be used as the normal baseline case.

The preliminary model confirmed that the geometry, contact method and output requests worked. It showed that D2 had to be selected by reaction-force calibration rather than visual indentation depth.

3.4 Representative tractor, tyre, and vertical load basis

The modelled tyre was a Firestone Performer Extra / Performer 85 380/85R28 fitted to a John Deere 6330 tractor, which was used as the representative tractor-tyre case. The selected tyre size is listed in Firestone data as 380/85R28, with load index 133D / 130E. Load index 133 corresponds to a rated vertical capacity of approximately 2060 kg per tyre. The equivalent rated vertical force is:

$$F_{rated} = mg$$

$$F_{rated} = 2060 \times 9.81 = 20208.6\ N$$

$$F_{rated} \approx 20.2\ kN$$

(Eq. 3)

The full rated load was not used as the baseline because it represented a high-limit tyre capacity rather than a typical front-wheel transport condition. The target vertical load was therefore derived by scaling from Becker and Els (2022), who tested a Trelleborg TM700 280/70R16 tyre, load index 112, under 5.68 kN.

$$F_{LI112} = 1120 \times 9.81 = 10987.2\ N$$

$$F_{LI112} \approx 10.99\ kN$$

(Eq. 4)

The Becker and Els test load therefore represented:

$$\frac{5.68}{10.99} = 0.517$$

$$0.517 \times 100 = 51.7\%$$

(Eq. 5)

Applying the same proportion to the selected Firestone tyre gave the baseline target vertical load:

$$F_{baseline} = 0.517 \times 20.2$$

$$F_{baseline} = 10.44\ kN$$

(Eq. 6)

A baseline vertical reaction target of approximately 10.5 kN per front tyre was therefore selected. This provided a literature-linked agricultural tyre load basis while avoiding the use of the tyre's full rated capacity as the default simulation condition.

The previously used vertical displacement value, D2 = -2.8 mm, had produced an approximate vertical reaction of 22.06 kN during early simulation development. This value is higher than the Firestone LI133 rated load basis:

$$\frac{22.06}{20.2} = 1.092$$

$$1.092 \times 100 = 109.2\%$$

(Eq. 7)

Therefore, D2 = -2.8 mm was treated only as a solver-development and exploratory overload case. Final simulations used D2 calibration to select an indentation close to the 10.5 kN target.

Table 2 Vertical load basis used for simulation planning

Case	Basis	Target vertical reaction per tyre	Use in project
Lower load sensitivity	Light front axle / lower transport condition	8.9 kN	Optional sensitivity
Baseline	Becker and Els scaled proportion	10.5 kN	Main comparison
Upper load sensitivity	Heavier front axle / ballast uncertainty	12.5 kN	Optional sensitivity
Severe case	80% of LI133 rated tyre load	16.2 kN	Optional severe sensitivity
Early D2 = -2.8 mm case	Solver-development result	22.06 kN	Exploratory / overload only

3.5 Vertical displacement calibration

D2 was calibrated by running a short displacement-reaction sweep around the 10.5 kN target. The exported SPCF reaction forces were summed for each trial displacement. This calibration was required because the model was displacement-controlled, D2 set tread indentation while the summed SPCF reaction determined whether the load case was representative.

Table 3 Vertical displacement calibration against the 10.5 kN baseline reaction target

Trial D2 value	Summed SPCF reaction	Difference from 10.5 kN target	Decision
-2.1 mm	5.11 kN	-51.3%	Too low
-2.2 mm	10.54 kN	+0.4%	Selected baseline
-2.3 mm	15.91 kN	+51.5%	Too high

The selected baseline indentation was D2 = -2.2 mm, producing approximately 10.54 kN. This was close to the 10.5 kN target. The sweep showed a non-linear response because increasing D2 from -2.2 mm to -2.3 mm greatly increased reaction force, supporting calibration by reaction rather than visual judgement.

3.6 Simulation test matrix

After the baseline vertical indentation was calibrated, the final comparison was arranged as a paired simulation matrix. The purpose of the matrix was to ensure that standard and reversed tyre orientation were compared under matched geometry, material, friction, road and loading assumptions. The only intended difference between the two main cases was the direction of the imposed longitudinal scrub relative to the lug geometry.

Table 4 Final baseline simulation test matrix

Case ID	Orientation	D2 vertical indentation	Achieved vertical reaction	D1 horizontal scrub	Coefficient of friction	Purpose
S-BL	Standard	-2.2 mm	10.54 kN	-3.0 mm	0.80	Baseline standard-orientation case
R-BL	Reversed	-2.2 mm	10.54 kN	+3.0 mm	0.80	Baseline reversed-orientation case

Optional sensitivity cases were identified during planning, but they were only included in the results where completed solver output was available. The main comparison was therefore based on the paired baseline cases shown in Table 4.

3.7 Final material assumptions

The exact Firestone tread compound was not available. Tyre manufacturers do not normally publish full rubber recipes or complete constitutive data for commercial agricultural tyres. The early model therefore used a simplified near-incompressible elastic tread material to establish solver behaviour before the final material assumptions were checked.

Agricultural tyre tread lugs are physically manufactured from a vulcanized polymer matrix comprising blends of Natural Rubber (NR) for high tensile tear and chip resistance, and Styrene-Butadiene Rubber (SBR) to provide mechanical protection against road surface abrasion (Plaschka *et al*., 2025). While real vulcanized tread rubber demonstrates complex, non-linear viscoelastic and hyper-elastic behaviour under dynamic rolling conditions, a representative macroscopic isotropic elastic formulation was selected for this comparative geometric study. The rubber compound was configured with an equivalent Young's Modulus of E = 7.5 MPa. This value was selected as a representative elastic stiffness for the simplified comparative model and was used consistently between standard and reversed cases. (Becker and Els, 2022; Sakhnevych and Genovese, 2024).

To enforce the bulk volume conservation characteristics inherent to solid elastomer compounds, the Poisson's ratio of the material was defined as nu = 0.49. Setting the Poisson's ratio close to the theoretical incompressibility limit of 0.50 is a common finite element modelling approach for representing rubber-like volume conservation under contact loading (Gent, 2012; Licher *et al*., 2023). Restricting the value to 0.49 provides a critical numerical regularisation that prevents volumetric locking within the solid first-order tetrahedral elements used to mesh the lug, which would otherwise induce artificial structural stiffness and distort the interface contact traction results. The rigid road block was defined as an unyielding steel-grade surface proxy with a Young's

Modulus of E = 210 GPa and a Poisson's ratio of nu = 0.30. This effectively isolates the elastomeric lug as the sole deforming body within the tribological interface.

3.8 Displacement-controlled loading method

The model used enforced displacement rather than applied force as the main control method. This was chosen because non-linear contact models are more stable when contact is established progressively. It allowed the same displacement path to be applied to the standard and reversed cases, leaving orientation as the controlled variable.

The simulation used two sequential load steps. Loadstep 1 displaced the tread vertically into the road to form contact. Loadstep 2 displaced the compressed tread horizontally to impose braking scrub. Separating the stages avoided applying vertical indentation and scrub at the same instant, which would not represent the physical sequence of lug entry followed by shear.

$$Loadstep\ 1: compression\ /\ indentation\ \rightarrow\ Loadstep\ 2: horizontal\ scrub$$

The imposed vertical displacement was labelled D2. D2 was not interpreted as a physical tyre deflection by itself. It was used as a numerical control input, and its suitability was judged by the vertical reaction force produced at the support nodes. The reaction extraction was defined as:

$$F_z = \sum_{i=1}^{n} R_{z,i}$$

(Eq. 8)

where F_z is the total vertical reaction force, R_z,i is the vertical reaction at node i, and n is the number of support nodes included in the extraction.

The imposed horizontal displacement was labelled D1. It was used as a local scrub distance, not as a wheel-slip percentage. The final scrub input was set to ±3 mm because it was small enough to represent local tread scrub rather than gross sliding, but large enough to produce measurable differences in the contact outputs.

$$D1_standard = -3.0\ mm$$

$$D1_reversed = +3.0\ mm$$

The same vertical indentation, material card, contact settings, road block and output method were retained between the two orientations. The sign of D1 was changed to reverse the direction of local scrub across the lug geometry. Subcase continuity was used so that the horizontal scrub stage inherited the contact state from the vertical indentation stage. In the OptiStruct setup this was handled using non-linear continuation settings such as CNTNLS = YES where applicable.

3.9 Mesh, road proxy and contact setup

The tread geometry was meshed using first-order tetrahedral solid elements, with local refinement at the tread-road contact face and coarser elements in the upper support region. This mesh strategy was selected because contact traction, contact pressure and contact force outputs are sensitive to element quality and local contact discretisation. Coarser elements were retained away from the contact interface to reduce computational cost in regions where lower stress gradients were expected.

Figure 7 shows the meshed local tread-strip model used for the final standard and reversed simulations. The model included the reconstructed tread section and a fixed high-stiffness road block. The same mesh was retained for both orientation cases, with the reversed condition produced by changing the imposed horizontal scrub direction rather than by re-meshing the geometry.

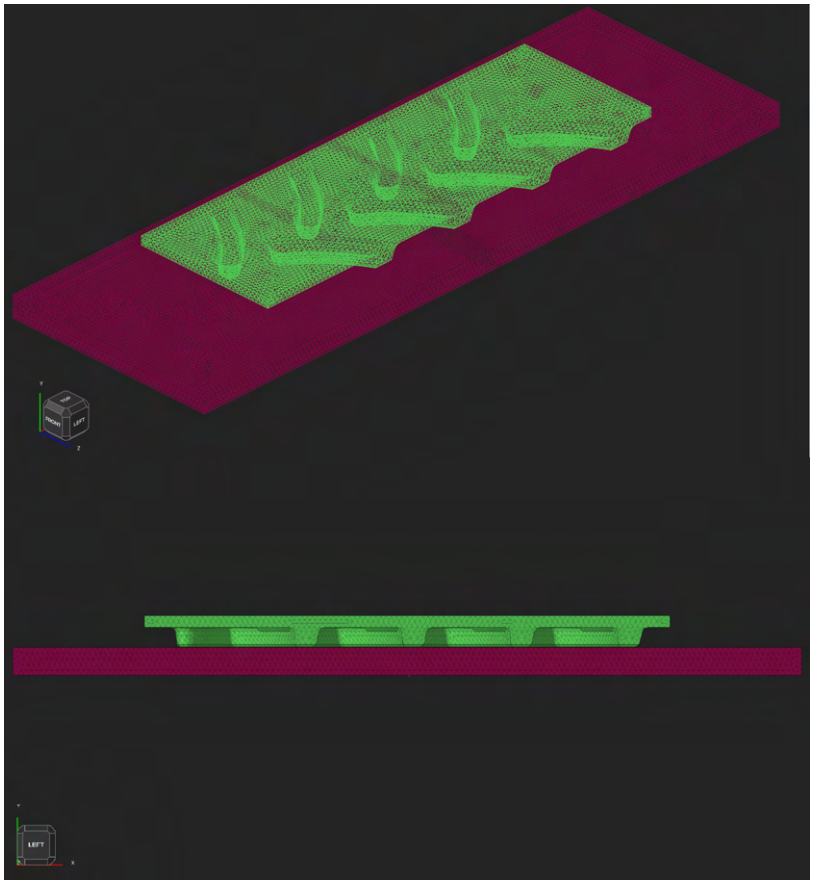


Figure 7 Finite element mesh of the local tread-strip contact model: (a) overall mesh layout showing the tread strip and fixed road proxy; (b) side view showing the lug geometry and tread-road contact interface. Source: Author.

The road block was treated as a high-stiffness hard-surface proxy, with E = 210 GPa. This was selected because the project scope concerned agricultural tractor movement on hard non-deformable surfaces, including paved roads and concrete yards. The model did not attempt to reproduce asphalt micro-texture, concrete roughness, aggregate geometry or thermomechanical road behaviour. Including these effects would have increased simulation complexity and reduced control over the standard-versus-reversed comparison.

3.10 Contact formulation and friction model

The tread-road interaction was modelled using non-linear surface-to-surface contact. The contact formulation allowed regions of the tread to open, close, stick, or slip depending on the local normal and tangential contact state.

The friction model used a Coulomb law:

$$\tau_{crit} = \mu P$$

(Eq. 9)

where:

- τ_{crit} is the limiting tangential shear stress before local sliding;
- μ is the coefficient of friction;
- P is the local normal contact pressure.

The coefficient of friction was set to represent dry rubber-road contact. The coefficient of friction was set to:

$$\mu = 0.80$$

for all final standard and reversed simulations. This was treated as an assumed dry rubber-road contact value rather than a tyre-specific measured coefficient for the Firestone tread compound. The value was therefore used to maintain a consistent comparative contact condition between orientations, not to claim an exact field-calibrated friction response.

The contact output was interpreted using the following logic:

- Closed stick indicated regions where contact existed but relative tangential motion had not exceeded the friction limit.
- Closed slip indicated regions where the tread-road interface was undergoing local sliding.
- Open contact indicated regions not currently in contact.
- Tangential traction indicated local shear intensity at the interface.
- Tangential contact force provided an additional nodal-force-based comparison of tangential response.

The Contact Status plot was used to identify sliding regions. It was not used as a general masking tool for all traction and force plots unless the same masking workflow was applied consistently to both standard and reversed cases.

3.11 Solver and contact settings

Final simulations used OptiStruct non-linear static analysis because the model required contact opening/closing, stick-slip transition and local tread deformation under imposed displacement. Solver settings were kept consistent so differences could be attributed to orientation and scrub direction.

Table 5 Solver and contact settings used for the final simulations.

Setting	Final setup
Pre-processor	Altair HyperMesh
Solver	OptiStruct
Analysis type	non-linear static
CNTNLS	YES
Contact formulation	Surface-to-surface tread-road contact
Friction law	Coulomb friction
Coefficient of friction	μ = 0.80
Road constraint	Road block fixed
Tread loading method	Enforced displacement
Loadstep 1	Vertical indentation, D2 = -2.2 mm
Loadstep 2	Horizontal scrub, D1 = ±3.0 mm
Main outputs	Contact Status; Contact Traction/Tangent (Mag); Contact Force/Tangent (Mag); SPCF reaction
Comparison control	Same material, mesh, road, friction and D2 settings used for both orientations

3.12 Model verification checks

Verification checks confirmed that the simplified model was suitable for a controlled relative comparison. They did not validate it as a full tyre-life prediction model.

Both final baseline cases achieved numerical convergence in the OptiStruct non-linear static solution. The two sequential load steps were solved in the same order for both simulations: LOADSTEP_1_COMPRESS applied the vertical indentation, and LOADSTEP_2_SLIDE applied the horizontal scrub displacement after contact had been established. This was important because applying horizontal scrub before stable contact formation would have reduced the reliability of the contact-state comparison.

The road block was constrained using single-point constraints so that it acted as a fixed hard-surface proxy. Visual inspection of the deformation and contact plots confirmed that the road did not translate or rotate during the solution. Contact was checked using the Contact Status output. Active contact was confined to the intended lug-road interface, with no visible spurious contact patches elsewhere in the model.

The same calibrated D2 = -2.2 mm was applied to both cases, producing approximately 10.54 kN. Horizontal scrub then used equal and opposite D1 values: -3 mm for standard and +3 mm for reversed.

The standard and reversed simulations used the same mesh, material properties, friction coefficient, road constraint, load-step sequence and output requests. The reversed condition was produced by changing the direction of the imposed horizontal displacement rather than by re-meshing or physically mirroring the CAD geometry. This reduced the risk of mesh-density or element-shape differences influencing the comparison.

Post-processing was controlled between the two cases. The same result frames were used for comparison: Frame 1 represented the end of the vertical compression load step, while Frame 2 represented the end of the horizontal scrub load step. Comparative plots for Contact Status, tangential contact traction and tangential contact force were displayed using common legend limits where possible, so that differences in colour distribution reflected differences in the model response rather than changes in the plotting scale.

Only routine non-linear solver warnings were observed. These included minor negative eigenvalue warnings and automatic time-step bisection during contact engagement. These warnings were consistent with a nearly incompressible elastomeric contact model using nu = 0.49 and high friction sliding contact. The final converged results were therefore retained, but the warnings were considered when interpreting highly localised peak values. For this reason, the results were interpreted using contact distribution patterns and comparative trends rather than isolated single-node maxima.

Table 6 Verification checks applied to the final baseline simulations.

Verification check	Method used	Outcome
Solver convergence	Review of final non-linear solution status for both baseline cases	Standard and reversed cases converged
Road constraint	Visual inspection of deformation and constraint behaviour	Road block remained fixed
Contact location	Contact Status output reviewed at compression and scrub stages	Contact occurred at the intended lug-road interface
Vertical load calibration	Summed SPCF reaction from the calibrated D2 sweep	D2 = -2.2 mm produced approximately 10.54 kN
Matched vertical loading	Same (D_2) applied to standard and reversed cases	Vertical loading held constant
Matched scrub magnitude	Equal and opposite (D_1) values applied	Standard: -3 mm, reversed: +3 mm
Material consistency	Same rubber material values used in both models	E = 7.5 MPa, nu = 0.49
Friction consistency	Same Coulomb friction coefficient used in both models	mu = 0.80
Mesh consistency	Scrub direction changed without re-meshing	Same node and element structure retained
Post-processing consistency	Same frames and contour legend ranges used	Direct visual comparison supported
Solver warnings	non-linear warnings reviewed	No fatal errors; warnings treated as interpretation limitations

3.13 Wear-severity theory and output selection

The model did not calculate material removal. Outputs were selected because they related to wear-severity variables.

Classical abrasive wear is often introduced through Archard's wear expression:

$$W = K\frac{Ps}{H}$$

(Eq. 10)

where:

- W is wear volume or wear amount;
- K is a wear coefficient;
- P is normal pressure or normal load term depending on formulation;
- s is sliding distance;
- H is hardness of the softer material.

For the present comparison, the wear coefficient, hardness, material model, and imposed sliding-distance magnitude were held constant between standard and reversed cases. Therefore, the

model did not use Archard's law to calculate absolute wear. Instead, it used the law as a framework for identifying why pressure, sliding, and tangential contact action are relevant to wear.

More recent tyre-wear literature links local wear to frictional work or frictional power. Local frictional power density may be written as:

$$\dot{w}_f = \tau_t \cdot v_{slip}$$

(Eq. 11)

where:

- $\dot{w}_f$ is local frictional power density;
- τ_t is local tangential traction;
- v_{slip} is local sliding velocity.

The cumulative frictional work density over a contact interval may then be expressed as:

$$w_f = \int_{t_1}^{t_2} \tau_t \cdot v_{slip} dt$$

(Eq. 12)

For a simplified imposed-displacement model, the exact local sliding velocity field is not fully resolved in the same way as in a rolling tyre simulation. However, because the imposed horizontal displacement magnitude is equal and opposite between the two orientations, the tangential traction distribution remains a useful comparative wear-severity indicator. Where a derived frictional work-style index is used, it should be treated as a relative index rather than a calibrated physical wear value.

A simplified local frictional work index may therefore be defined as:

$$I_w = \tau_t \mid D1 \mid$$

(Eq. 13)

where:

- I_w is the relative local frictional work index;
- τ_t is tangential contact traction;
- $\mid D1 \mid$ is the imposed horizontal scrub displacement magnitude.

Since $\mid D1 \mid$ is the same for the standard and reversed cases, differences in I_w are controlled mainly by differences in the local tangential traction field.

3.14 Output extraction and comparison method

The final sliding frame was used for comparison because it represented contact after both vertical compression and horizontal scrub.

Three primary outputs were extracted:

1. **Contact Status**
   Used to identify open, closed-stick, and closed-slip regions.
2. **Contact Traction / Tangent (Mag)**
   Used as the main local shear-stress-based wear-severity proxy.
3. **Contact Force / Tangent (Mag)**
   Used as an additional tangential contact response indicator, especially for identifying localised nodal force concentrations.

For each orientation, the following values were recorded:

$$\tau_{t,max}$$

$$F_{t,max}$$

$$F_{t,total} = \sum_{i=1}^{n} F_{t,i}$$

(Eq. 14)

where:

- $\tau_{t,max}$ is the maximum local tangential traction;
- $F_{t,max}$ is the maximum local tangential contact force;
- $F_{t,total}$ is the summed tangential contact force across selected contact nodes;
- $F_{t,i}$ is the tangential contact force at node i.

The comparison was based on both magnitude and distribution. A single maximum value can be affected by local mesh behaviour, so the contour pattern and location of high-shear regions were interpreted. Particular attention was given to whether high values concentrated on the leading or trailing edges of the lugs, because reversing the tyre changes which physical lug face receives the imposed scrub direction.

To avoid misleading visual interpretation, common legend scales were used wherever possible for standard and reversed contour plots. If different automatic legend scales were used by the post-processor, the numerical maximum and minimum values were recorded separately and not judged from colour alone.

3.15 Practical and ethical constraints

The project did not involve human participants, personal data, animal use, customer-owned destructive testing, or public-road experimental trials. The practical work was limited to workshop-based tyre footprint capture and computer-based finite element simulation. During footprint capture, the tractor was moved slowly in a controlled private workshop area, and the water-soluble paint method avoided permanent tyre damage.

A simulation-led method was selected for practical and ethical reasons. A full road-wear trial would have required extended public-road operation, repeated tyre measurement, control of weather and

road-surface variation, and deliberate tyre wear. That would have introduced poorer repeatability, increased practical risk and additional tyre-wear emissions. The simplified simulation method therefore reduced physical testing requirements while still allowing a controlled comparison of standard and reversed orientation under matched assumptions.

3.16 Methodology limitations

The first limitation is the local tread-strip representation. The model does not include a full pneumatic tyre, carcass, belt package, sidewall, bead constraint or air chamber. It therefore cannot represent full tyre deformation, rolling-radius change, cyclic lug entry and exit, or inflation-pressure variation.

The second limitation is the material model. The preliminary material was a placeholder elastic rubber and the final material model remains a simplified representation unless a calibrated hyper-elastic or viscoelastic tread compound is added. Real tyre rubber is affected by compound formulation, strain rate, temperature, ageing and damage history.

The third limitation is the hard-surface road proxy. The road block represents a stiff concrete/asphalt-type counter-surface but does not include measured asphalt micro-texture, concrete roughness, aggregate shape, water, debris or road temperature. These features are known to influence real rubber wear.

The fourth limitation is the imposed scrub input. D1 = ±3 mm gives a controlled local sliding input, but it is not a measured braking event and it does not reproduce full wheel rotation. The model can compare the response to equal and opposite local scrub directions, but it cannot predict a complete road-duty cycle.

The fifth limitation is wear prediction. No calibrated wear law was implemented, so the model cannot convert contact output into tread-depth loss, rubber mass loss, service life or mileage. The results should therefore be presented as relative wear-severity indicators only.

3.17 Methodology summary

The methodology developed a controlled local tread-road contact model for comparing standard and reversed orientation of a Firestone 380/85R28 agricultural front tyre. The model was built in stages. The preliminary simulations established that the two-loadstep contact method worked, that the required outputs could be extracted, and that the original D2 = -2.8 mm indentation produced an excessive vertical reaction of about 22.06 kN.

The final method retained the successful parts of the preliminary model but recalibrated the vertical indentation target around a representative 10.5 kN front-wheel reaction. Horizontal scrub was applied using equal and opposite D1 values of -3 mm and +3 mm. Contact Status, Contact Traction / Tangent (Mag) and Contact Force / Tangent (Mag) were used to compare local contact severity between the standard and reversed cases.

The method is suitable for a relative comparison of local wear-severity indicators under matched simplified conditions. It is not a full tyre-life prediction method. The results must therefore be discussed as evidence of changed contact response, not as proof of absolute tread-life improvement.

4. Results

4.1 Post-processing basis

Results were extracted from the final sliding stage of the non-linear static simulation. Unless otherwise stated, contour plots and numerical values refer to Frame 2, after vertical compression and horizontal scrub had been applied. Frame 1 plots were used only to show the compression-stage contact condition (Figure 8).

The numerical comparison used tread-side contact nodes only. The road component was excluded because it acted as a fixed high-stiffness counter-surface, while the project assessed tread wear-severity indicators.

4.2 Contact status

The Contact Status plots were used to check whether the standard and reversed cases reached the intended contact condition before the numerical contact outputs were compared. At Frame 1 (Figure 8), both cases had established contact between the tread lugs and road block. The contact area was mainly closed-stick, with limited local closed-slip regions around parts of the lug edges. This showed that the compression step formed a contact patch before the horizontal scrub displacement was applied.

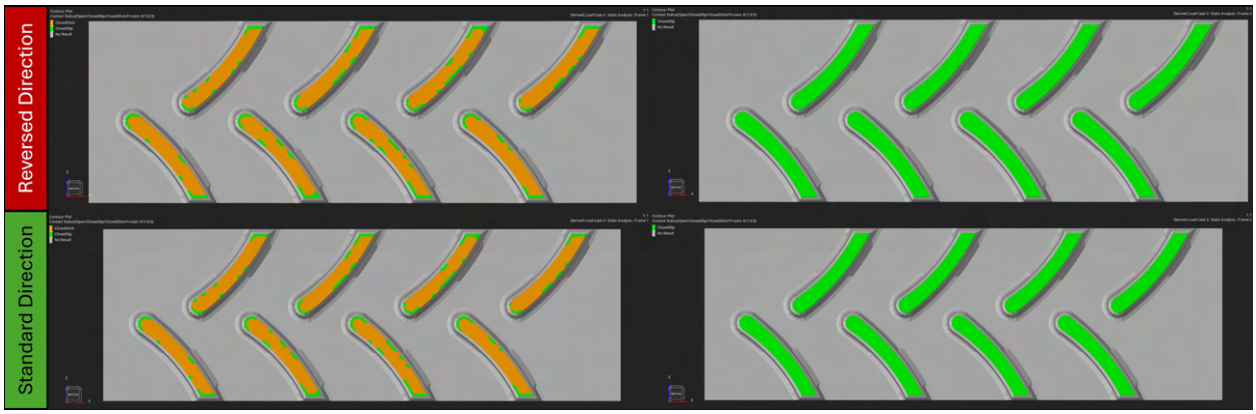


Figure 8 Contact status comparison for the standard and reversed tyre-orientation models: (Top Left) Frame 1; reversed orientation after compression, (Top Right) Frame 2; reversed orientation after horizontal scrub, (Bottom Left) Frame 1; standard orientation after compression, (Bottom Right) Frame 2; standard orientation after horizontal scrub. Source: Author.

At Frame 2 (Figure 8), the active contact areas in both orientations were shown as closed-slip. This confirmed that the final comparison was taken from the sliding stage rather than from the compression-only stage. The standard and reversed cases therefore reached the same type of contact condition before the tangential force and traction results were interpreted.

4.3 Numerical comparison of tread-side contact outputs

All values in this section were extracted from the tread-side contact nodes at the final sliding frame.

The standard orientation produced the higher peak tangential contact response. The maximum tread-side Contact Force / Tangent (Mag) was 8.537E-03 kN in the standard case and 7.747E-03 kN in the reversed case, giving a 9.25% reduction in the reversed orientation. The same trend was observed for Contact Traction / Tangent (Frictional Shear Mag), where the standard case reached 9.004E-05 GPa and the reversed case reached 7.697E-05 GPa, a reduction of 14.52%.

Mean and summed values showed much smaller differences. The summed Contact Force / Tangent (Mag) was 2.9109 kN for the standard case and 2.9036 kN for the reversed case, a difference of only 0.25%. The main change was therefore a reduction in local peaks rather than a large reduction in total contact loading.

The 95th percentile values supported this interpretation. The reversed case was lower for both tangential contact force and tangential traction, although the difference was smaller than the peak-value reduction.

Overall, the numerical results (Table 7) indicated that reversed orientation redistributed the tread-side contact response rather than removing tangential loading. It reduced the highest local wear-severity indicators but did not substantially reduce the total tangential contact-force sum.

Table 7 Tread-side numerical comparison of tangential contact force and tangential traction outputs at the final sliding frame.

Metric	**Standard**	**Reversed**	**Reversed vs standard**
Contact Force / Tangent max (kN)	8.537E-03	7.747E-03	-9.25%
Contact Force / Tangent mean (kN)	4.300E-03	4.289E-03	-0.25%
Contact Force / Tangent median (kN)	3.860E-03	4.032E-03	+4.46%
Contact Force / Tangent 95th percentile (kN)	7.021E-03	6.750E-03	-3.86%
Contact Force / Tangent sum (kN)	2.9109	2.9036	-0.25%
Contact Traction / Tangent max (GPa)	9.004E-05	7.697E-05	-14.52%
Contact Traction / Tangent mean (GPa)	4.722E-05	4.705E-05	-0.36%
Contact Traction / Tangent median (GPa)	4.719E-05	4.833E-05	+2.42%
Contact Traction / Tangent 95th percentile (GPa)	6.613E-05	6.492E-05	-1.82%

Figure 9 shows the tread-side Contact Traction / Tangent (Frictional Shear Mag) distribution at the final sliding frame. This output was used as the local shear-based wear-severity indicator. Both orientations showed shear response along the active lug faces, but the standard case produced the higher tread-side peak. This matched the numerical extraction in Table 7, where the standard case reached 9.004E-05 GPa compared with 7.697E-05 GPa for the reversed case.

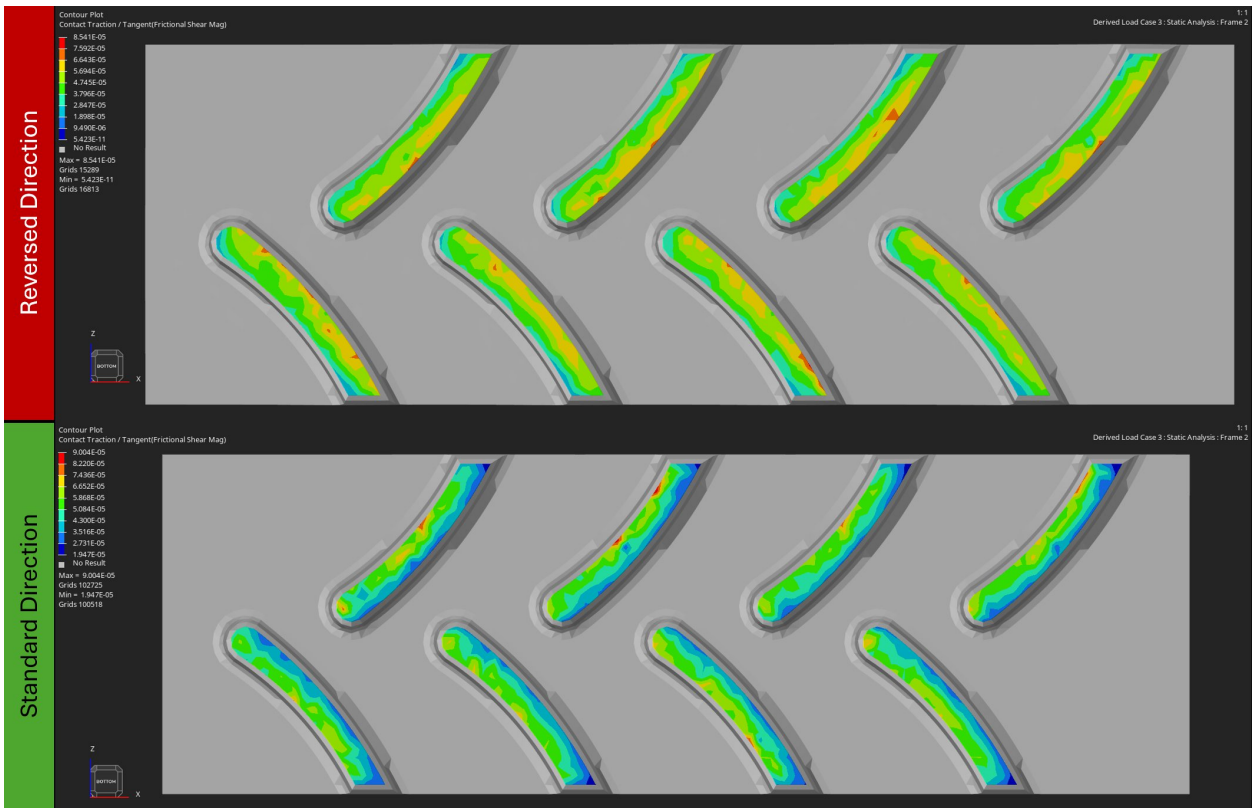


Figure 9 Tread-side Contact Traction / Tangent (Frictional Shear Mag) comparison at the final sliding frame: standard orientation; reversed orientation. Numerical comparison was based on exported tread-side values; contour plots show distribution pattern. Source: Author.

The traction contours supported the interpretation that reversal reduced the highest local shear-traction peak, but did not remove sliding contact from the tread-road interface. The broader contact paths remained similar, indicating redistribution of local severity rather than elimination of tangential contact.

Figure 10 shows the tread-side Contact Force / Tangent (Mag) distribution at the final sliding frame. Both cases showed tangential contact response along the active lug faces, but the standard case produced the higher local maximum. The numerical extraction confirmed this trend, with the standard case reaching 8.537E-03 kN compared with 7.747E-03 kN for the reversed case.

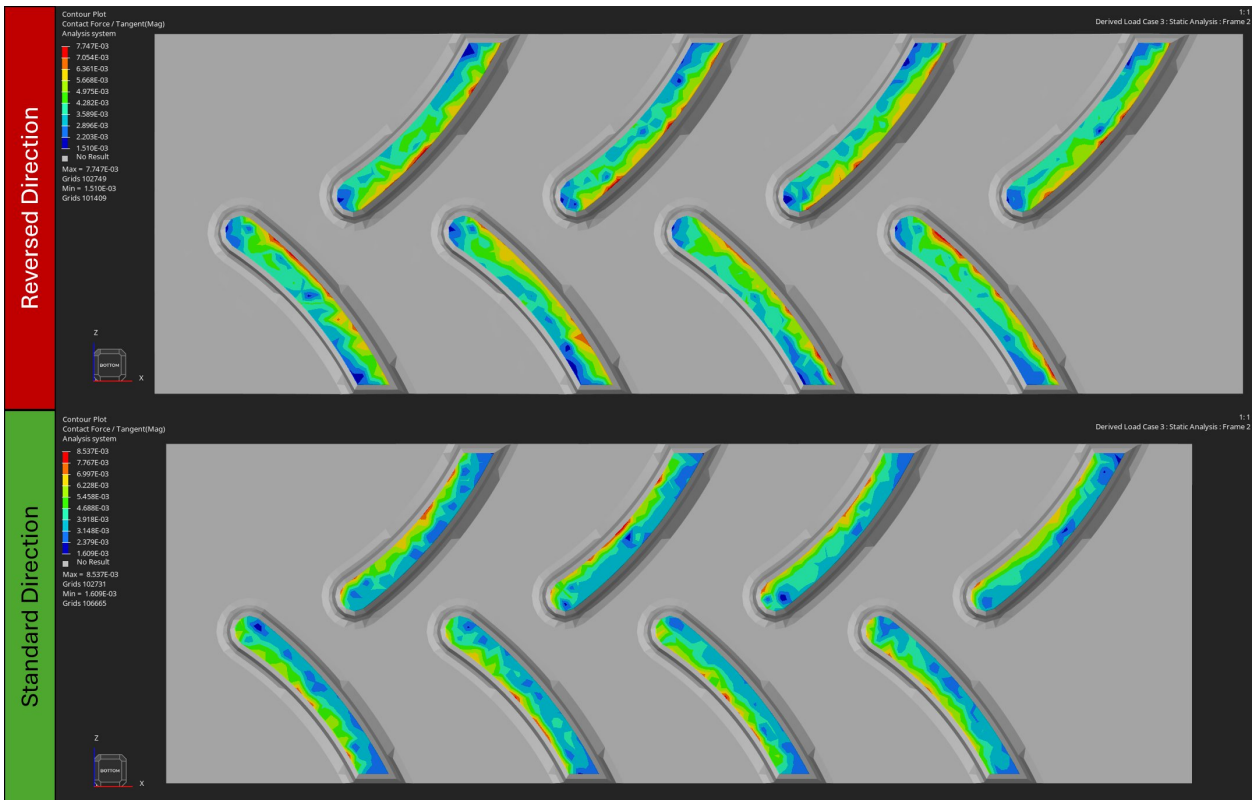


Figure 10 Tread-side Contact Force / Tangent (Mag) comparison at the final sliding frame: standard orientation; reversed orientation. Numerical comparison was based on exported tread-side values; contour plots show distribution pattern. Source: Author.

The contact-force contours showed that the reversed orientation reduced the highest local tangential force concentration while retaining a broadly similar overall contact path. This supported the numerical result that the summed tangential contact force changed very little between orientations, even though the peak value was lower in the reversed case.

4.4 Results summary

Results showed that reversing the tread orientation reduced the highest local tread-side peaks. The reversed case reduced the maximum tangential contact force by 9.25% and the maximum tangential traction by 14.52% compared with the standard case. However, the summed tangential contact force changed by only 0.25%, indicating that the overall tangential contact action was almost unchanged.

The main result was therefore not a clear reduction in total contact loading. Instead, reversed orientation reduced local severity peaks while leaving the general contact action broadly similar, supporting interpretation as a contact redistribution effect.

5. Discussion and evaluation

5.1 Interpretation against the research question

The project question was whether reversed agricultural front tyres reduced road wear compared with standard orientation. Results did not show a large reduction in total tangential contact action: summed Contact Force / Tangent (Mag) changed by only 0.25%, indicating that the overall tangential contact loading was almost unchanged between the standard and reversed cases. However, reversed orientation reduced peak Contact Force / Tangent (Mag) by 9.25% and peak Contact Traction / Tangent (Frictional Shear Mag) by 14.52%.

The most defensible interpretation was that reversal did not remove the wear mechanism, but reduced the most severe local tread-side peaks under the simulated braking-scrub condition. This indicated redistribution of local wear-severity indicators rather than a clear reduction in total wear energy or absolute material loss.

5.2 Relationship to the literature

The result agreed with the literature because tyre wear was controlled by local contact behaviour rather than global load alone. The literature review identified local pressure, sliding, tangential shear, frictional work, temperature and damage history as the main wear-governing variables. The standard and reversed cases had the same vertical loading and almost the same total tangential contact force, yet produced different local peak values.

The result aligned with the directional abrasion literature. Reversing the tyre changed which lug face acted as the leading or trailing face during the imposed scrub event. The reduction in peak tread-side tangential traction in the reversed case suggested that the orientation change altered the local shear history across the lug. However, the result did not prove that reversed tyres would last longer in service, because the model did not include repeated cycles, temperature rise, road texture, debris, steering inputs or measured rubber removal.

5.3 Engineering significance of the result

From an engineering viewpoint, the reversed case showed a useful reduction in local peak severity. This could help explain operator reports of more even front-tyre wear, because agricultural lugs often wear unevenly at edges and corners where local shear and pressure concentrate.

However, the small change in summed tangential contact force means the result should not be interpreted as a large reduction in total wear. The likely benefit of reversal was improved distribution of local severity rather than removal of the road-wear mechanism.

This affects the practical recommendation. Reversing a standard agricultural tyre may be a low-cost way to alter where severe local contact occurs, but it does not redesign the tyre for road transport. For tractors that spend a high proportion of time on hard surfaces, the more complete engineering solution may be to select or develop an agricultural tyre designed for mixed field and road duty. That claim was not tested directly in this project, so it is treated as a recommendation for further work rather than as a conclusion from the present results.

5.4 Validity of the simulation evidence

The comparison was strengthened by matched modelling. Both orientations used the same tread geometry, vertical indentation, material properties, friction coefficient, road proxy, mesh and output method; only horizontal scrub direction changed.

The Contact Status plots supported the comparison. Both cases reached comparable closed-slip contact conditions at the final frame, meaning that the force and traction outputs were compared at the same stage of the load sequence. This was important because comparing one case during sticking and another during sliding would have made the numerical comparison unreliable.

The main weakness was external validity. The model represented a simplified local tread-strip event, not a full rolling pneumatic tyre, and excluded carcass deformation, inflation-pressure variation, heat generation, road texture, ageing, steering duty, repeated cycles and a calibrated wear law. The results are therefore valid as a controlled comparison of local contact severity, but not as proof of tyre service-life improvement.

5.5 Limitations affecting interpretation

The material model was a major limitation. The tread used simplified near-incompressible elasticity rather than a calibrated Firestone compound. Real agricultural tread rubber is viscoelastic, temperature-dependent and damage-history dependent. This means the model could compare orientation but not predict real abrasion rate.

The road representation limited interpretation. The high-stiffness road block allowed the tread lug to act as the deforming body, which was suitable for a controlled comparison. However, real asphalt and concrete contain roughness, aggregate shape, moisture, debris and thermal variation. These factors affect friction and wear, so the model cannot represent all real road conditions.

The imposed scrub displacement was another limitation. The ±3 mm horizontal displacement provided a controlled local braking-scrub input, but it was not measured from an actual tractor braking event. The model therefore tested a plausible local contact mechanism rather than a complete road-duty cycle.

5.6 Project evaluation

The project succeeded in producing a controlled comparison between standard and reversed tyre orientation. The method was able to isolate orientation as the main variable and generate interpretable contact-status, tangential force and tangential traction outputs. This addressed the original problem more rigorously than relying on operator reports alone.

The project did not prove that reversed front tyres reduce total road wear or extend tyre life. The evidence was narrower: reversed orientation reduced peak local wear-severity indicators while leaving overall tangential contact action almost unchanged. This is still useful because it provides a mechanical explanation for why reversed tyres might wear more evenly, but it does not justify a broad claim of reduced total wear.

5.7 Recommendations for further work

Further work should focus on validation and improved physical realism. Useful next stages would include controlled physical wear test using rubber samples or tread sections under matched normal load, sliding distance and direction. The second improvement would be a full tyre or sector model with inflation pressure and carcass deformation, and field measurement of tread-depth change on a controlled road-duty route.

A further extension would be to compare reversed fitting against a road-suitable agricultural tyre. The present study compared only the same lugged agricultural tyre in standard and reversed orientation. A stronger practical study would compare three cases under the same load and scrub conditions: a standard lugged tyre, the same tyre reversed and a road-focused agricultural tyre designed for higher transport duty.

This comparison would test whether a road-duty tyre design would reduce both peak tread-side severity and total tangential contact action. The present results suggested that reversal mainly redistributed local severity, while leaving summed tangential contact force almost unchanged.

A calibrated wear law would still be needed before any model could estimate tread-depth loss, rubber mass loss or service life. Without that calibration, the most appropriate use of the current model is as an early-stage comparative tool for identifying changes in local contact severity.

6. Conclusion

This project investigated whether reversing agricultural front tyres reduced road wear compared with standard orientation. A simplified finite element contact model of a Firestone Performer Extra / Performer 85 380/85R28 tread section was used under matched hard-surface loading. The model did not predict service life, tread-depth loss or rubber mass removal; it compared local tread-side wear-severity indicators between standard and reversed orientations.

Reversed orientation did not substantially reduce overall tangential contact action. The summed Contact Force / Tangent (Mag) changed by only 0.25% between the standard and reversed cases, indicating that the same general road-wear mechanism remained in both orientations. Reversing the tyre therefore could not be concluded to reduce total road wear under the simulated condition.

However, the reversed orientation reduced the highest local tread-side contact peaks. Maximum Contact Force / Tangent (Mag) fell by 9.25%, and maximum Contact Traction / Tangent (Frictional Shear Mag) fell by 14.52%. These reductions suggest that reversing the tyre changed how the local contact severity was distributed across the lug geometry. The most defensible conclusion is therefore that reversed orientation acted as a wear-redistribution mechanism, not a clear total-wear reduction mechanism.

This provided a possible mechanical explanation for operator reports that reversed-front-tyre wear more evenly during road transport. If the highest local shear and force peaks are reduced, the tread may experience less severe local edge loading. However, because the model excluded repeated rolling cycles, temperature rise, real road texture, carcass deformation, inflation-pressure effects and a calibrated wear law, it could not prove improved tyre life.

The project produced a controlled comparison by keeping geometry, material assumptions, vertical load, friction coefficient, road proxy and output method constant while changing only horizontal scrub direction. This allowed the effect of orientation to be isolated more clearly than would be possible from uncontrolled field observations alone.

Overall, reversed agricultural front tyres did not show a clear reduction in total road-wear loading in the model, but they did reduce peak local wear-severity indicators. Reversed fitting may therefore redistribute local tread severity, but should not be treated as a proven road-wear solution. Further work should compare standard, reversed and road-suitable agricultural tyre designs using validated wear testing or a more complete tyre-road model.

Reference list

Ally, H., Wang, X., Wu, T., Liu, T. and Ge, J. (2025) ‘Improving agricultural tire traction performance through finite element analysis and semi-empirical modelling’, *Eng*, 6(4), article 63. Available at: https://doi.org/10.3390/eng6040063 (Accessed: 17 June 2026).

Altair (2026a) *non-linear static analysis*. Available at: https://help.altair.com/hwsolvers/os/topics/solvers/os/analysis_non-linear_quasi_static_c.htm (Accessed: 17 June 2026).

Altair (2026b) *SPCD*. Available at: https://help.altair.com/hwsolvers/os/topics/solvers/os/spcd_bulk_r.htm (Accessed: 17 June 2026).

Becker, C. and Els, S. (2022) ‘Agricultural tyre stiffness change as a function of tyre wear’, *Journal of Terramechanics*, 102, pp. 1–15. Available at: https://doi.org/10.1016/j.jterra.2022.04.001 (Accessed: 17 June 2026).

Braghin, F., Cheli, F., Melzi, S. and Resta, F. (2005) ‘Sensitivity analysis of the tyre design parameters with respect to tyre wear using a physical tyre model’, *Vehicle System Dynamics*, 43(sup1), pp. 102–110. Available at: https://doi.org/10.1080/00423110500109034 (Accessed: 17 June 2026).

Cho, J.R., Choi, J.H. and Kim, Y.S. (2011) ‘Abrasive wear amount estimate for 3D patterned tire utilizing frictional dynamic rolling analysis’, *Tribology International*, 44(7–8), pp. 850–858. Available at: https://doi.org/10.1016/j.triboint.2011.02.007 (Accessed: 17 June 2026).

Dassault Systèmes (2025) *Inserting and resizing sketch pictures*. Available at: https://help.solidworks.com/2025/english/solidworks/sldworks/t_insert_and_resize_pictures.htm (Accessed: 17 June 2026).

Farroni, F. and Sakhnevych, A. (2022) ‘Tire multiphysical modeling for the analysis of thermal and wear sensitivity on vehicle objective dynamics and racing performances’, *Simulation Modelling Practice and Theory*, 117, article 102517. Available at: https://doi.org/10.1016/j.simpat.2022.102517 (Accessed: 17 June 2026).

Firestone Agriculture (2026) *Performer Extra 85 technical data*. Available at: https://www.firestone-agriculture.eu/en/technical-datasheets/firestone-performer-extra-85 (Accessed: 17 June 2026).

Gent, A.N. (2012) *Engineering with rubber: How to design rubber components*. 3rd edn. Munich: Hanser. Available at: https://doi.org/10.3139/9783446428713 (Accessed: 17 June 2026).

Giechaskiel, B., Ferrarese, C. and Grigoratos, T. (2025) ‘Tire wear, tread depth reduction, and service life’, *Vehicles*, 7(2), article 29. Available at: https://doi.org/10.3390/vehicles7020029 (Accessed: 17 June 2026).

Huang, M., Guibert, M., Thévenet, J., Fayolle, C., Chaussée, T., Guy, L., Vanel, L., Loubet, J.-L. and Sotta, P. (2018) 'A new test method to simulate low-severity wear conditions experienced by rubber tire materials', *Wear*, 410–411, pp. 72–82. Available at: https://doi.org/10.1016/j.wear.2018.06.004 (Accessed: 17 June 2026).

John Deere (2018) *Use mechanical front wheel drive (MFWD)*. Available at: http://manuals.deere.com/omview/OMLVU28456_19/JZ81662,0000FBD_19_20130225.html (Accessed: 17 June 2026).

Kane, M. and Cerezo, V. (2015) 'A contribution to tire/road friction modeling: From a simplified dynamic frictional contact model to a "Dynamic Friction Tester" model', *Wear*, 342–343, pp. 163–171. Available at: https://doi.org/10.1016/j.wear.2015.08.007 (Accessed: 17 June 2026).

Licher, J., Schmerwitz, F., Soleimani, M. and Junker, P. (2023) 'Experimental investigation of the tire wear process using camera-assisted observation assessed by numerical modeling', *Tribology International*, 189, article 108918. Available at: https://doi.org/10.1016/j.triboint.2023.108918 (Accessed: 17 June 2026).

Liu, C. and Cebon, D. (2025) 'Characterizing wear performance of tyre tread rubber', *Wear*, 566–567, article 205754. Available at: https://doi.org/10.1016/j.wear.2025.205754 (Accessed: 17 June 2026).

Marques Filho, A.C., Santana, L.S., Martins, M.B., Guimarães Júnnyor, W. da S., Medeiros, S.D.S. de and Lanças, K.P. (2025) 'Straw cover and tire model effect on soil stress', *AgriEngineering*, 7(8), article 263. Available at: https://doi.org/10.3390/agriengineering7080263 (Accessed: 17 June 2026).

Moore, D.F. (1972) *The friction and lubrication of elastomers*. Oxford: Pergamon Press.

Nguyen, V.H., Zheng, D., Schmerwitz, F. and Wriggers, P. (2018) 'An advanced abrasion model for tire wear', *Wear*, 396–397, pp. 75–85. Available at: https://doi.org/10.1016/j.wear.2017.11.009 (Accessed: 17 June 2026).

Plaschka, E.H., Akutagawa, K., Di Federico, E. and Busfield, J.J.C. (2025) 'Developing a more representative friction and wear simulator for tire tread compounds', *Polymer Testing*, 143, article 108688. Available at: https://doi.org/10.1016/j.polymertesting.2025.108688 (Accessed: 17 June 2026).

Sakhnevych, A. and Genovese, A. (2024) 'Tyre wear model: A fusion of rubber viscoelasticity, road roughness, and thermodynamic state', *Wear*, 542–543, article 205291. Available at: https://doi.org/10.1016/j.wear.2024.205291 (Accessed: 17 June 2026).

The Farming Forum (2016) *Reversed front tyres*. Available at: https://thefarmingforum.co.uk/index.php?threads/reversed-front-tyres.114926/ (Accessed: 17 June 2026).

Tires Easy (2023) Galaxy EarthPro Radial R-1W 480/80R50 159D. Available at: https://www.tires-easy.com/480-80-50/galaxy-tires/earthpro-radial-r-1w/tirecode/494663 (Accessed: 5 July 2026).

Vieira, T., Ferreira, R.P., Kuchiishi, A.K., Bernucci, L.L.B. and Sinatora, A. (2015) 'Evaluation of friction mechanisms and wear rates on rubber tire materials by low-cost laboratory tests', *Wear*, 328–329, pp. 556–562. Available at: https://doi.org/10.1016/j.wear.2015.04.001 (Accessed: 17 June 2026).

Wriggers, P. (2006) *Computational contact mechanics*. 2nd edn. Berlin: Springer. Available at: https://doi.org/10.1007/978-3-540-32609-0 (Accessed: 17 June 2026).

Yadav, R. and Raheman, H. (2024) 'A machine learning-based approach for estimation of deflection and contact area characteristics of tubeless and tube-type agricultural tyres', *Engineering Applications of Artificial Intelligence*, 133(Part D), article 108357. Available at: https://doi.org/10.1016/j.engappai.2024.108357 (Accessed: 17 June 2026).

Zhang, M., Unrau, H.-J., Gießler, M. and Gauterin, F. (2025) 'Tire tread wear characteristics: Insights from indoor experiments and analytical modeling', *Tribology International*, 210, article 110752. Available at: https://doi.org/10.1016/j.triboint.2025.110752 (Accessed: 17 June 2026).